PAPER

Resistive switching mechanism of MoS_2 based atomristor

To cite this article: Xiao-Dong Li *et al* 2023 *Nanotechnology* **34** 205201

IOP Publishing Nanotechnology
Nanotechnology 34 (2023) 205201 (8pp) https://doi.org/10.1088/1361-6528/acb69d

Resistive switching mechanism of MoS_2 based atomristor

Xiao-Dong Li, Bai-Qian Wang, Nian-Ke Chen* and Xian-Bin Li*

State Key Laboratory of Integrated Optoelectronics, College of Electronic Science and Engineering, Jilin University, 130012 Changchun, People's Republic of China

E-mail: chennianke@jlu.edu.cn and lixianbin@jlu.edu.cn

Received 28 October 2022, revised 15 January 2023
Accepted for publication 27 January 2023
Published 28 February 2023

Abstract

The non-volatile resistive switching process of a MoS_2 based atomristor with a vertical structure is investigated by first-principles calculations. It is found that the monolayer MoS_2 with a S vacancy defect (V_S) could maintain an insulation characteristic and a high resistance state (HRS) is remained. As an electrode metal atom is adsorbed on the MoS_2 monolayer, the semi-conductive filament is formed with the assistance of V_S. Under this condition, the atomristor presents a low resistance state (LRS). The ON state current of this semi-filament is increased close to two orders of magnitude larger than that without the filament. The energy barrier for an Au-atom to penetrate the monolayer MoS_2 via V_S is as high as 6.991 eV. When it comes to a double S vacancy (V_{S2}), the energy barrier is still amounted to 3.554 eV, which manifests the bridge-like full conductive filament cannot form in monolayer MoS_2 based atomristor. The investigation here promotes the atomic level understanding of the resistive switching properties about the monolayer MoS_2 based memristor. The physics behind should also work in atomristors based on other monolayer transition-metal dichalcogenides, like WSe_2 and $MoTe_2$. The investigation will be a reference for atomristor-device design or optimization.

Supplementary material for this article is available online

Keywords: atomristor, monolayer MoS_2, non-volatile resistive switching, 2D materials, memristor, defect

(Some figures may appear in colour only in the online journal)

1. Introduction

In the past ten years, various kinds of non-volatile memory [1–7] with excellent performances are developed for advanced applications, such as in-memory computing technology [8–10], which is an important strategy to possibly solve the famous von Neumann bottleneck in data-intensive industry [11, 12]. Among these newly-developing components, resistive random-access memory (RRAM) has emerged as a leading contestant owing to its simply vertical metal–insulator–metal (MIM) architecture as well as high-density storage ability [13].

Compared to traditional devices, two-dimensional material based memristors, which possess the distinctive characteristics of layered materials [14, 15], are anticipated to be shrunken in dimensions and ease of integration. Recently, the non-volatile resistance switching (NVRS) effect have been demonstrated in a single layer MoS_2 [a kind of transition-metal dichalcogenides (TMDs)] or hexagonal boron nitride (*h*-BN) stuck in the middle of metal electrodes with a vertical structure [16–18]. It was considered impossible within a time owning to the dilemma of retaining insulating properties [16]. The memristor devices based on atomically thin monolayer two-dimensional materials are also called as atomristors [17], which could promote a further miniaturization of newly-developing memory and computing devices. Differing from the preceding multi-layer two-dimensional material based RRAMs, where conductive channels were possibly formed with assistance by grain boundaries [19–21], how to form a conductive filament in an atomristor is yet confused. Because of this, improving the cycle-to-cycle and device-to-device

* Authors to whom any correspondence should be addressed.

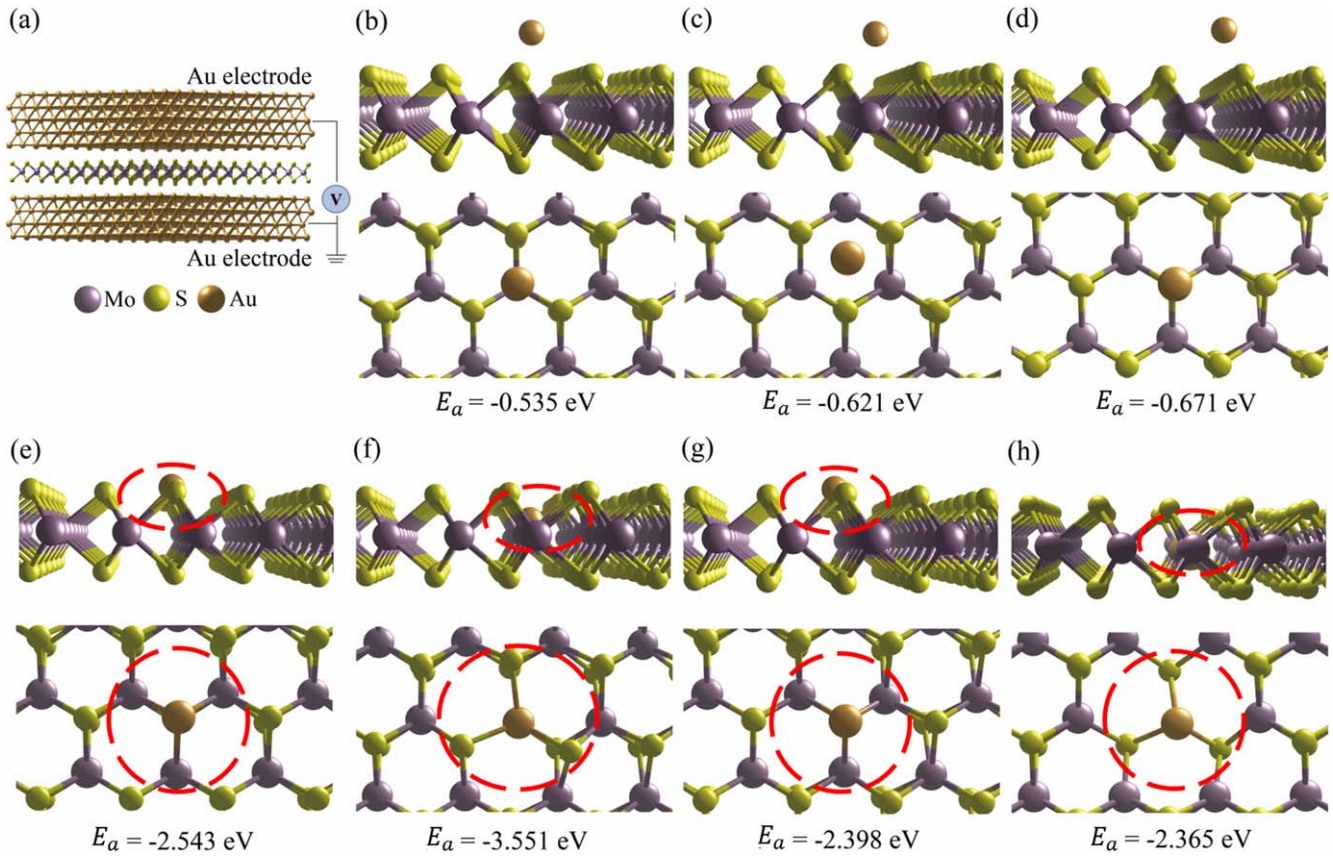

Figure 1. (a) The schematic of a MoS_2 based atomristor device with metal electrodes. (b)–(d) Au atom adsorbed on pristine MoS_2 atomic sheet: above (b) Mo site, (c) honeycomb, (d) S site. (e)–(h) Structures of MoS_2 with Au adsorption on (e) V_S, (f) V_{Mo}, (g) V_{S2}, and (h) V_{MoS3}. In each case, the side view and top view are shown. The red circles indicate the vacancy position with Au adsorbed.

Table 1. The formation energies of different vacancies in monolayer MoS_2.

Formation energy (eV)	S-rich	Mo-rich
V_S	2.649 eV	1.089 eV
V_{S2}	5.227 eV	2.107 eV
V_{Mo}	4.818 eV	7.939 eV
V_{MoS3}	6.871 eV	5.311 eV

inconsistency is still a significant challenge for these atomically thin devices [16, 17]. Though the origin of the NVRS process in MoS_2 based atomristors has been considered to be related to the electrode atoms adsorbed on TMD [22], whether the atoms could penetrate a MoS_2 atomic sheet to form a bridge-like full conductive filament is still unknown.

In this study, first-principles calculations [23, 24] associated with Keldysh nonequilibrium Green's function (NEGF) theory [25] are adopted to simulate the atomic migration process and electronic transport properties in a MoS_2 based atomristor with a MIM structure. The results manifest the resistive switching behavior in this atomic device is originated from the dissociation-adsorption process of electrode atoms on V_S. The conductive channel formed at low resistance state (LRS) is a semi-filament rather than a full filament going across the MoS_2 layer. The switching process should be also applicable in the other TMDs (such as WSe_2 and $MoTe_2$) based atomristors. The investigation here will promote the comprehension of these devices at atomic scale and be a reference for the device design or optimization.

2. Computational methods

Vienna *ab initio* simulation package (VASP) [26] is employed to carry out energy related calculations. The Nudged elastic band (NEB) [27] method is taken to evaluate the energy barriers for Au atom passing through the MoS_2 monolayer. Perdew, Burke and Ernzerhof functional is chosen to account the interaction of electron exchange and correlation [28]. A 7×7 supercell is built for the monolayer MoS_2 sheet, the cutoff energy is set to 500 eV. The k-points for structure optimization and density of states calculations are $3 \times 3 \times 1$ and $5 \times 5 \times 1$, respectively. The residual forces convergence criteria for structure relaxation and energy-barrier calculations are 0.01 eV·Å^{-1} and 0.05 eV·Å^{-1}, respectively. The energy is considered to be converged as two consecutive steps with an energy variation less than 10^{-6} eV.

The nonequilibrium quantum transport properties are investigated by Nanodcal [29]. To simplify the model for reducing large calculation demand, metal atom chains replace plane electrodes (as seen in figure S1 in supporting information) when *I*–*V* curves are evaluated. In calculating

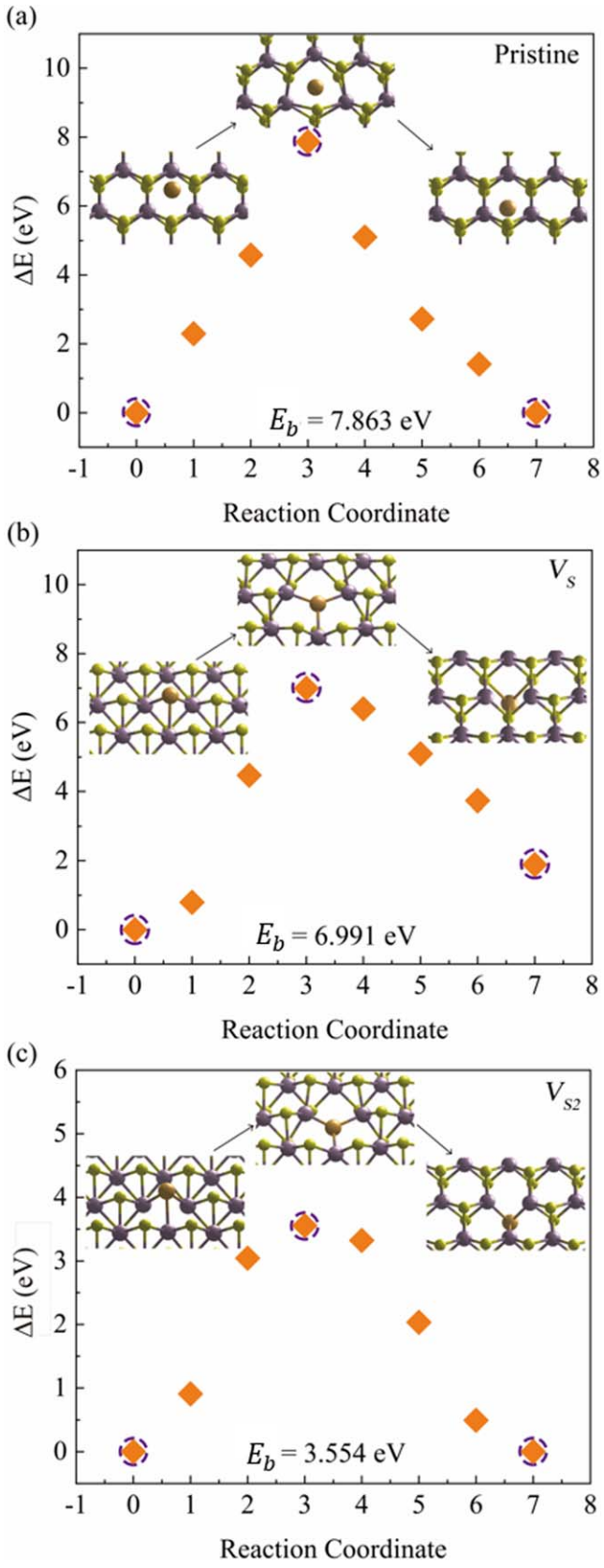

Figure 2. The E_b for an Au-atom penetrating the (a) single layer MoS_2 without defect, and MoS_2 with (b) V_S or (c) V_{S2} defect. The points marked by purple dash circles indicate the energies of initial, transition, final states as displayed in corresponding structural snapshots in the insets.

processes, double-zeta polarized atomic orbital basis is adopted [30]. Atomic potentials are described by standard norm-conserving nonlocal pseudopotentials [31]. The 80 Hartree cutoff and 100 × 100 × 1 k-points are set. The 100 K electronic temperature is used to set the electron occupation via Fermi–Dirac distribution.

3. Results and discussions

Figure 1(a) presents the schematic picture of a MoS_2 based atomristor. In fact, such an atomically thin non-volatile memory has been successfully demonstrated in a recent experiment [17]. According to previous research results, we choose Au as the electrodes likewise. Generally, electrode atoms tend to be adsorbed on monolayer MoS_2 under the electric field [18]. In this process, the Fermi level (E_F) of MoS_2 could be altered and therefore it is important for the resistive behavior, as seen in figure S2. For evaluating the influences in its entirety, the structures of MoS_2 with Au adsorption are exhibited in figure 1. The method to calculate the adsorption energy (E_a) is as below:

$$E_a = E_{\mathrm{Au+MoS_2}} - E_{\mathrm{Au}} - E_{\mathrm{MoS_2}}, \tag{1}$$

where $E_{\mathrm{Au+MoS_2}}$ is the energy of pristine/defective MoS_2 with Au adsorption, $E_{\mathrm{MoS_2}}$ is the pristine/defective MoS_2 energy, E_{Au} is the energy of an isolated Au atom. Figures 1(b)–(d) show the various adsorption states of Au atom on pristine MoS_2. We can see that an Au atom just can be adsorbed weakly on MoS_2 without defect since the E_a is between −0.535 and −0.671 eV only. Hence, pristine monolayer MoS_2 without defects can hardly provide a precondition for forming non-volatile conductive channels. On the contrary, adsorption of an Au atom on V_S, V_{Mo}, V_{S2} and V_{MoS3} defects (Here, V_{MoS3} is for that a Mo atom and its surrounding three S atoms are absent) are much more stable, and the E_a is −2.365 ∼ −3.551 eV as seen in figures 1(e)–(h). Side/top views of these adsorbed structures are shown as well. In our model, the two S vacancies in a V_{S2} defect locate at opposite sides which is in consistent with the experimentally observed V_{S2} defect in monolayer MoS_2 [22, 32]. The results indicate that Au atom can be chemisorbed on defective MoS_2 stably, which may provide a possibility of realizing a conductive nonvolatility in the atomristor. Based on the above results, it can be inferred that the formation of conductive filaments in monolayer MoS_2 is probably related to vacancies. This explains why the resistive switching behavior cannot be observed on defect-free areas in an experimental report [22]. In consideration that the large-size defects (such as multi-vacancy) will bring about an accumulation of metal atoms and cause a failure of short circuit in device cells [33], therefore we mainly focus on the mentioned small-size defects.

Then defect formation energy in single layer MoS_2 is calculated by the equations [34]:

$$E_f = E_{\mathrm{def}} - E_{\mathrm{tot}} + \sum n_i \mu_i \tag{2}$$

$$\mu_{\mathrm{Mo}} + 2 \times \mu_S = \mu_{\mathrm{MoS_2}} \tag{3}$$

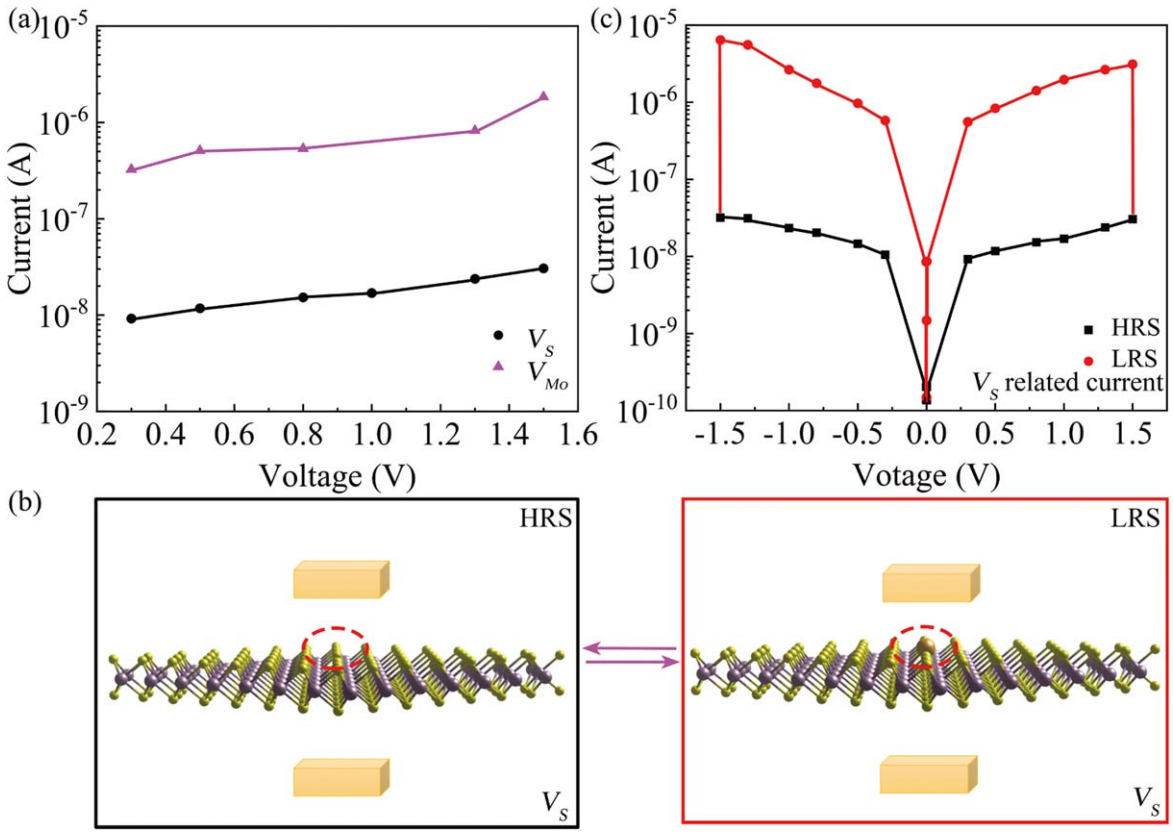

Figure 3. (a) Calculated *I*–*V* curves of defective MoS_2 with V_S and V_{Mo}, respectively. (b) Schematics of MoS_2 based atomristor without filament (left) and with a semi-filament (right). The orange blocks schematically represent electrodes. (c) Simulated *I*–*V* curves of MoS_2 atomristor.

Table 2. Calculated current of V_{S2}/V_S without and with Au adsorption at 0.5 V.

Condition	Current at 0.5 V	State
V_{S2}	8.3766×10^{-10} A	HRS
Au-V_{S2}	4.7319×10^{-8} A	LRS
V_S	1.1753×10^{-8} A	HRS
Au-V_S	8.3504×10^{-7} A	LRS

where E_f is the formation energy, E_{def} is the energy of a defective MoS_2 supercell, E_{tot} is the pristine MoS_2 energy with the same size of the supercell. The n_i and μ_i are the counts and chemical potential of atom i being doped or removed in the system, respectively. Equation (3) restricts a scope for the permissible values of the chemical potentials for S and Mo atoms, within restriction about their sum under the thermal equilibrium state. In this research, the S and Mo chemical potentials at their respective rich conditions were chosen as the energy of each atom of the orthorhombic bulk α-S (solid) and the body-centered cubic bulk Mo (solid), respectively. μ_{MoS_2} is the energy per unit of pristine MoS_2. As seen in table 1, compared to V_{Mo} and V_{MoS3}, V_S and V_{S2} defects with lower formation energies should be the dominant intrinsic defects in monolayer MoS_2, which is consistent with a previous experimental observation [32]. Therefore, we mainly focus on V_S and V_{S2} defects for further discussions. In fact, these two kinds of defects were indeed mainly observed in the experiment [22].

The adsorption of Au atoms on monolayer MoS_2 with vacancies provides a possibility of forming conductive filaments, but whether bridge-like filaments like the case in monolayer *h*-BN [33] could form in MoS_2 based atomristor is still unclear. Usually, in the switching process, metal atoms of electrode are inclined to transfer along the direction of electric field. Hence, the formation of bridge-like conductive filaments in atomristors should be accompanied with migrations of Au atoms, which is not easily observed through experimental methods. Then, the difficulty level that an Au atom penetrates the single layer MoS_2 is required to be investigated. To come up with a feasible migration path of the metal atom, energy barriers (E_b) for an Au atom penetrating the MoS_2 monolayer at different conditions are simulated. The E_b for an Au atom penetrating the pristine MoS_2 is 7.863 eV [figure 2(a)], which is a very high barrier. With regards to the defective MoS_2, the E_b for Au atom going through is decreased as seen in figures 2(b)–(c). But the E_b for Au atom going through MoS_2 via V_S is 6.991 eV [figure 2(b)], and the one for the case of V_{S2} is still as high as 3.554 eV [figure 2(c)]. Therefore, the bridge-like conductive filaments are not able to be formed through V_S or V_{S2} because of the high enough E_b. When further enlarging the size of defect, the E_b for an Au atom going through the MoS_2 via V_{MoS3} can be lowered to 1.683 eV, which is still a relatively high barrier. In addition,

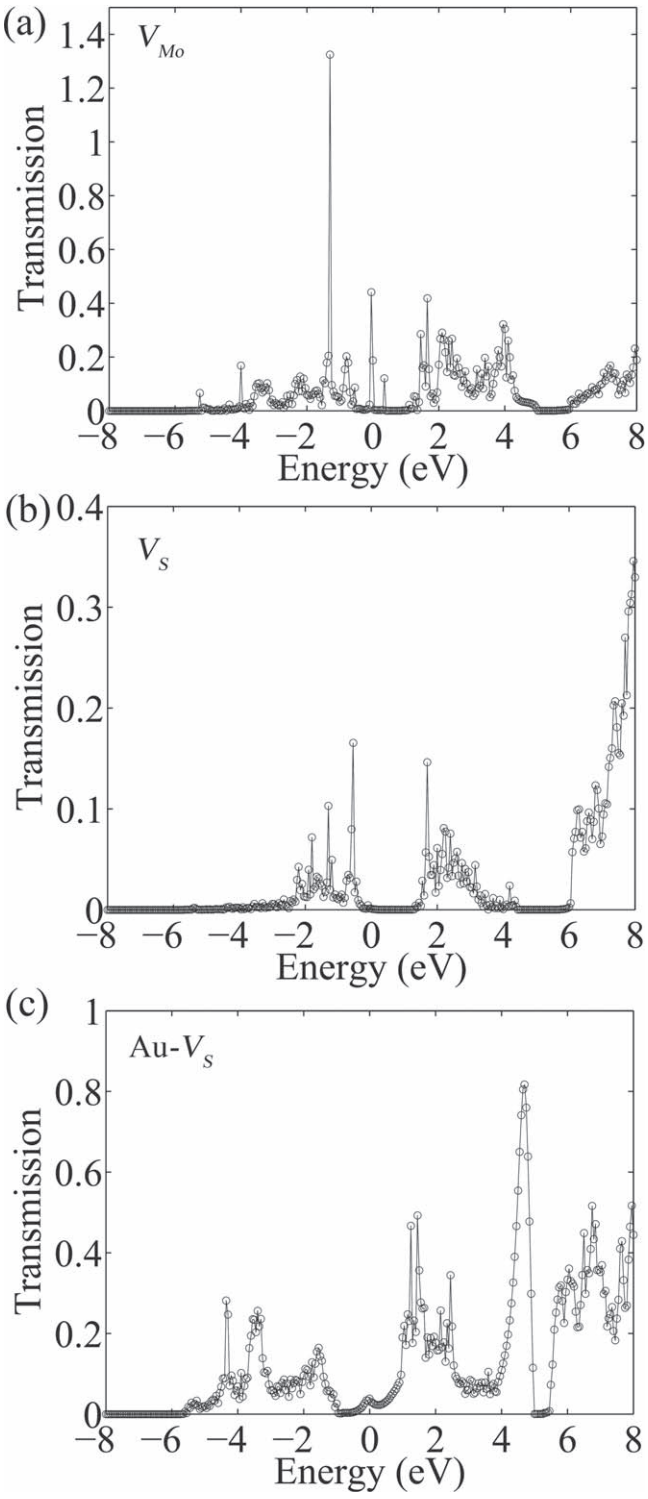

Figure 4. Transmission coefficient versus electron energy at zero-bias in defective monolayer MoS_2 with (a) V_{Mo}, (b) V_S and (c) Au adsorbed V_S, respectively. The Fermi levels are at 0 eV.

the formation energy of V_{MoS3} in monolayer MoS_2 is significantly higher than that of monovacancy, which makes it less likely to be produced in the growth process. In fact, V_{MoS3} was seldom observed experimentally in both chemical vapor deposition growth and exfoliated monolayer MoS_2 [17, 22, 32]. Therefore, unlike the bridge-like full-filament formed in the single layer *h*-BN based memristor [33], the forming of conductive channel under control of applied voltages in MoS_2 atomristor should be a kind of semi-filament without an Au penetration-migration process. This is consistent with a recent experimental observation [22].

To further comprehend the resistive switching mechanisms in the atomristor, Keldysh nonequilibrium Green's function and density functional theory (NEGF-DFT) quantum transport method is employed to simulate the *I–V* characteristics of the monolayer MoS_2 atomristor. The *I–V* curves of defective monolayer MoS_2 are calculated first. Simulation results in figure 3(a) manifest the single layer MoS_2 with V_S could still maintain an insulation characteristic with low current, while monolayer MoS_2 with V_{Mo} shows an insufficient insulation characteristic which means relatively large leakage current and thus blocks its application for RRAMs. Hence, V_{Mo} should be reduced in MoS_2 based atomristors. Considering the high resistance state (HRS) of the MoS_2 based atomristor as fabricated [17], we mainly focus on V_S defect below. In terms of experimental observations, V_S is indeed the dominant defect in monolayer MoS_2 [17, 32]. Figure 3(b) displays the atomristor without/with an Au-atom adsorption onto V_S of monolayer MoS_2 and figure 3(c) presents the calculated *I–V* curves of these structures. We can see that when the conductive filament is not existing (i.e. no Au absorption), the atomristor is set to HRS. Once the conductive channel is formed via Au adsorption, the cell is turned to LRS. The ON state current of this semi-filament is increased close to two orders of magnitude larger than that without filament (HRS). That is to say, the MIM structures with and without Au-atom adsorption can be the ON and OFF states of this atomically thin device. In fact, adsorption and desorption processes of Au atoms were indeed observed experimentally on the surface of monolayer MoS_2 [22]. The ON/OFF ratio calculated here is close to two orders of magnitude, and is larger than that of the experimental observation [22]. This is probably caused by the low current compliance limit which was set in the experiment as the setting will result in a lower ON state current. We should note that the V_{S2} vacancy could also provide a signal contrast by Au adsorption as shown in table 2. However, the LRS current related to V_{S2} is much lower compared to that of V_S, indicating a higher conductive ability of the Au-V_S semi-filament in the devices comparing to the case of the Au-V_{S2} semi-filament. Hence, we mainly discuss the conductive behavior about V_S.

To elucidate the characteristic of defects in resistive behaviors, transmission coefficients of defective MoS_2 (at zero bias) versus electron energy were analyzed. As shown in figures 4(a) and (b), there is a significant difference of transmission coefficient between the two configurations around Fermi level. For the case of V_{Mo}, there is an obvious transmission peak at Fermi level. While for the case of V_S, there is no evident transmission peak at Fermi level. This could explain the significant leakage current observed in the V_{Mo} based monolayer MoS_2, as calculated in figure 3(a). It also explains why the V_S based MoS_2 could maintain a good insulation property. Additionally, when an Au atom is adsorbed on V_S, it can be found that there is a noticeable

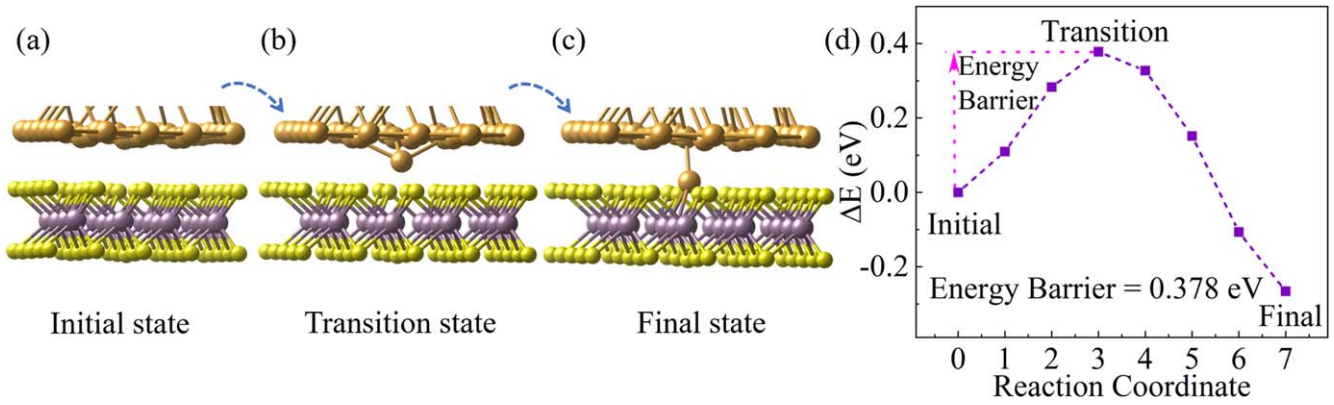

Figure 5. The simulated process and energy barrier of an Au atom dissociating from top electrode and being adsorbed on the V_S vacancy. The atomic pictures of the (a) initial state, (b) transition state and (c) final state. (d) Energy landscape of the process.

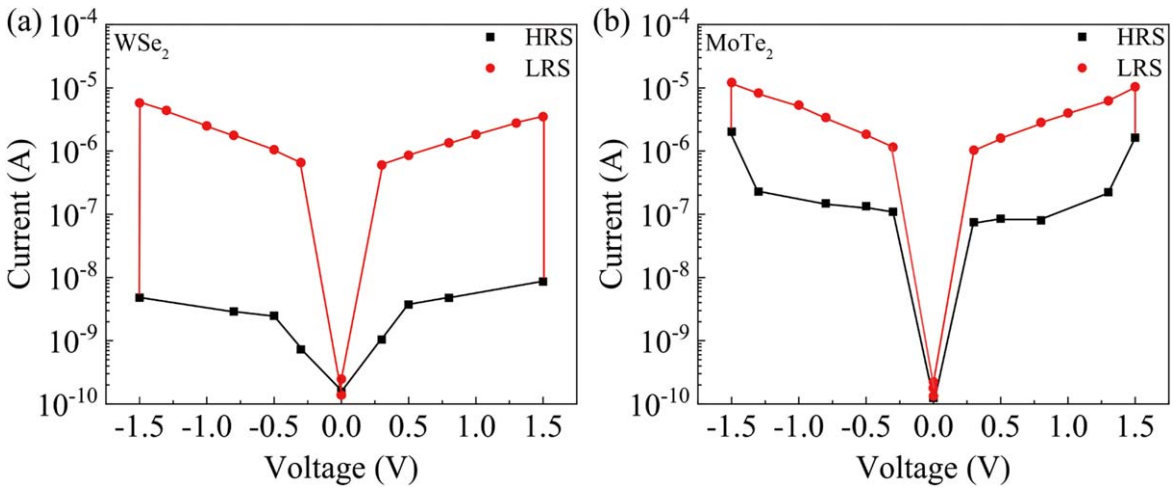

Figure 6. Simulated *I–V* curves of other monolayer TMD based atomristors based on the Au-V_{anion} conductive mechanism: (a) WSe_2 and (b) $MoTe_2$.

Table 3. The calculated current ON/OFF ratio of different monolayer TMD based atomristors at 0.5 V due to forming the Au-$V_{S/Se/Te}$ semi-filament.

Atomristors based on different TMDs	Current ON/OFF ratio at 0.5 V
MoS_2	71
WSe_2	229
$MoTe_2$	19

transmission peak appearing at E_F, as seen in figure 4(c). Hence, the Au adsorption process related to V_S could indeed enhance the conductivity in out-of-plane direction of monolayer MoS_2. The calculated structures of RESET (HRS) and SET (LRS) states are also presented in figure S1. It can be clearly seen that the conductive channel is a kind of semi-filament.

Next, the formation process of a semi-filament is presented with a simplied model in figure 5. At initial state, the monolayer MoS_2 is in HRS without Au adsorption [as seen in figure 5(a)]. As the Au atom dissociates from the surface of the top electrode [see figure 5(b)], the Au atom tends to interact with a nearby V_S defect and be adsorbed on it. Then, a semi-filament is formed, i.e. the final state as seen in figure 5(c). The energy barrier for this process is also calculated using the NEB method, which is reasonably as low as 0.378 eV [as seen in figure 5(d)] indicating the dissociation and adsorption processes would happen under the action of the electric field.

Motivated by the NVRS mechanism proposed above based on monolayer MoS_2, another two examples of monolayer TMDs including WSe_2 and $MoTe_2$ are further investigated and their atomristor *I–V* switching behaviors are also demonstrated in figure 6. In these two cases, Au atoms can also be adsorbed on WSe_2 and $MoTe_2$ stably via V_{Se} and V_{Te} with adsorption energies of −2.556 eV and −3.213 eV, respectively. Unsurprisingly, the calculated E_b for an Au atom penetrating the TMD monolayer with V_X (V_{Se}, V_{Te}) are still high: 5.260 eV for WSe_2 and 3.617 eV for $MoTe_2$. As shown in table 3, the atomristor based on monolayer WSe_2 have a lager ON/OFF ratio than those of $MoTe_2$ and MoS_2. As the absorption process of Au atoms, monolayer $MoTe_2$ has a larger adsorption energy (−3.213 eV) than MoS_2 (−2.543 eV) and

WSe_2 (−2.556 eV) do. However, $MoTe_2$ monolayer with Te vacancies is reported to undergo phase transitions with external stimuli such as laser exposure [35, 36]. Hence, considering the Au-atom absorption mechanism, the $MoTe_2$ based atomristor may not be stable enough. As for the electronic properties, monolayer WSe_2 have a lager current ON/OFF ratio compared to that of MoS_2 (as seen in table 3), indicating WSe_2 may be a better choice for non-volatile atomristor applications. These results manifest that the semi-filament mechanism proposed here should be also possibly applied in atomristors based on other monolayer TMDs.

We should note that, in vertical-structure memristors based on 2D materials, the grain boundaries could also play an important role in the formation of conductive filaments, especially for the cases of multi-layered 2D materials [19–21]. In this study, we mainly focus on the point-defect-related mechanism because previously reported memristors based on monolayer MoS_2 use the single-crystalline samples [17], and it has been found the point defects play a significant role in those devices [22]. Also, the memristor based on point defects in single-crystalline monolayer 2D materials is good for developing the memristor technology with an ultrahigh integration density and low power consumption. The grain boundaries in monolayer 2D materials can also influence the performance of memristor/atomristor, which is an important subject and worth further studying. On the other hand, the monolayer MoS_2 based memristor with different electrodes [37] may have different performances, whether the device with other electrodes will possess a better performance is an important issue and worth investigating in the future. Compared to the typical memristors based on bulk or film materials (such as the prototype metal/oxides/metal memristor) [38, 39], the thickness of atomristor studied in this work could be scaled down to atomic scale. Compared to the memtransistor based on 2D materials [40, 41], the monolayer 2D materials based vertical memristor devices with the simple MIM structures are of preference owing to the smaller footprint and denser integration [17].

4. Conclusion

In this research, the non-volatile resistive switching mechanism of MoS_2 based atomristor is investigated by DFT calculations combined with NEGF transport theory. It was found that the monolayer MoS_2 with V_S could maintain an insulating characteristic along out-of-plane direction, so a HRS is remained. When Au atom is adsorbed on atomic sheet with V_S, the semi conductive filament is formed and thus a LRS can be presented. The ON state current of this semi-filament is increased close to two orders of magnitude larger than that without the filament (OFF state). That is qualitatively consistent with the previous experimental result [22]. The energy barrier for an Au atom penetrating the monolayer MoS_2 via V_S is as high as 6.991 eV. When it comes to V_{S2}, the energy barrier is still amounted to a large value of 3.554 eV, which manifests the bridge-like full conductive filaments, happening in monolayer *h*-BN, cannot form in the MoS_2 based atomristor. The semi-filament proposed in the MoS_2 atomristor means a lower ON/OFF ratio than that of monolayer *h*-BN memristor [33]. However, owing to the lack of penetration process, the switching operation in MoS_2 atomristor should be easier to be controlled. That may be a reason why the monolayer MoS_2 based memristor has a better endurance and a lower SET voltage than that of the *h*-BN atomristor [17, 42]. At present stage, the endurance of the monolayer MoS_2 based memristor is just hundreds of cycles, which no doubt needs further improvements in future for practical applications. In addition, our results suggest that the performance of the atomristor could be optimized if Mo vacancies can be reduced by defect engineering. Two other TMD samples including WSe_2 and $MoTe_2$ are testified to be able to work in a similar NVRS mechanism. The work here exhibits a critical atomic picture of NVRS mechanism in TMD based memristors at their ultrathin limit, which may benefit the developments of the high-density integration RRAM technology.

Acknowledgments

This work was supported by the National Natural Science Foundation of China (Grant Nos. 12274172, 61922035, 12274180 and 11874171) and the China Postdoctoral Science Foundation (No. 2019M661200). This work was also supported by the Fundamental Research Funds for the Central Universities. The High-Performance Computing Center (HPCC) at Jilin University for computational resources is also acknowledged.

Data availability statement

The data generated and/or analysed during the current study are not publicly available for legal/ethical reasons but are available from the corresponding author on reasonable request.

Data availability statement

All data that support the findings of this study are included within the article (and any supplementary files).

ORCID iDs

Xian-Bin Li https://orcid.org/0000-0002-0046-2016

References

[1] Chen N K, Li X B, Bang J, Wang X P, Han D, West D, Zhang S and Sun H B 2018 Directional forces by momentumless excitation and order-to-order transition in

peierls-distorted solids: the case of GeTe *Phys. Rev. Lett.* **120** 185701
[2] Li X B, Liu X, Liu X, Han D, Zhang Z, Han X, Sun H B and Zhang S 2011 Role of electronic excitation in the amorphization of Ge-Sb-Te alloys *Phys. Rev. Lett.* **107** 015501
[3] Huang Y T, Chen N K, Li Z Z, Li X B, Wang X P, Chen Q D, Sun H B and Zhang S 2021 Mexican-hat potential energy surface in two-dimensional III_2-VI_3 materials and the importance of entropy barrier in ultrafast reversible ferroelectric phase change *Appl. Phys. Rev.* **8** 031413
[4] Wang S, Liu L, Gan L, Chen H, Hou X, Ding Y, Ma S, Zhang D W and Zhou P 2021 Two-dimensional ferroelectric channel transistors integrating ultra-fast memory and neural computing *Nat. Commun.* **12** 53
[5] Zhang Y *et al* 2021 Evolution of the conductive filament system in HfO_2-based memristors observed by direct atomic-scale imaging *Nat. Commun.* **12** 7232
[6] Wang M *et al* 2018 Robust memristors based on layered two-dimensional materials *Nat. Electron.* **1** 130–6
[7] Jiang T T, Wang X D, Wang J J, Zhang H Y, Lu L, Jia C, Wuttig M, Mazzarello R, Zhang W and Ma E 2022 *In situ* characterization of vacancy ordering in Ge-Sb-Te phase-change memory alloys *Fundam. Res.* (https://doi.org/10.1016/j.fmre.2022.09.010)
[8] Ielmini D and Wong H S P 2018 In-memory computing with resistive switching devices *Nat. Electron.* **1** 333–43
[9] Migliato Marega G, Zhao Y, Avsar A, Wang Z, Tripathi M, Radenovic A and Kis A 2020 Logic-in-memory based on an atomically thin semiconductor *Nature* **587** 72–7
[10] Xu X, Ding Y, Hu S X, Niemier M, Cong J, Hu Y and Shi Y 2018 Scaling for edge inference of deep neural networks *Nat. Electron.* **1** 216–22
[11] Stone H S 1970 A logic-in-memory computer *IEEE Trans. Comput.* **c-19** 73–8
[12] Chen W H *et al* 2019 CMOS-integrated memristive non-volatile computing-in-memory for AI edge processors *Nat. Electron.* **2** 420–8
[13] Sangwan V K and Hersam M C 2020 Neuromorphic nanoelectronic materials *Nat. Nanotechnol.* **15** 517–28
[14] Wang D, Li X B, Han D, Tian W Q and Sun H B 2017 Engineering two-dimensional electronics by semiconductor defects *Nano Today* **16** 30–45
[15] Xie S Y, Wang Y and Li X B 2019 Flat boron: a new cousin of graphene *Adv. Mater.* **31** 1900392
[16] Wu X, Ge R, Chen P A, Chou H, Zhang Z, Zhang Y, Banerjee S, Chiang M H, Lee J C and Akinwande D 2019 Thinnest nonvolatile memory based on monolayer h-BN *Adv. Mater.* **31** 1806790
[17] Ge R, Wu X, Kim M, Shi J, Sonde S, Tao L, Zhang Y, Lee J C and Akinwande D 2018 Atomristor: nonvolatile resistance switching in atomic sheets of transition metal dichalcogenides *Nano Lett.* **18** 434–41
[18] Ge R *et al* 2021 A library of atomically thin 2D materials featuring the conductive-point resistive switching phenomenon *Adv. Mater.* **33** 2007792
[19] Pan C *et al* 2017 Coexistence of grain-boundaries-assisted bipolar and threshold resistive switching in multilayer hexagonal boron nitride *Adv. Funct. Mater.* **27** 1604811
[20] Shi Y *et al* 2018 Electronic synapses made of layered two-dimensional materials *Nat. Electron.* **1** 458–65
[21] Li Y, Loh L, Li S, Chen L, Li B, Bosman M and Ang K W 2021 Anomalous resistive switching in memristors based on two-dimensional palladium diselenide using heterophase grain boundaries *Nat. Electron.* **4** 348–56
[22] Hus S M, Ge R, Chen P A, Liang L, Donnelly G E, Ko W, Huang F, Chiang M H, Li A P and Akinwande D 2021 Observation of single-defect memristor in an MoS_2 atomic sheet *Nat. Nanotechnol.* **16** 58–62
[23] Hohenberg P and Kohn W 1964 Inhomogeneous electron gas *Phys. Rev.* **136** B864
[24] Kohn W and Sham L J 1965 Self-consistent equations including exchange and correlation effects *Phys. Rev.* **140** A1133
[25] Jauho A P, Wingreen N S and Meir Y 1994 Time-dependent transport in interacting and noninteracting resonant-tunneling systems *Phys. Rev. B* **50** 5528
[26] Kresse G and Furthmüller J 1996 Efficiency of *ab-initio* total energy calculations for metals and semiconductors using a plane-wave basis set *Comput. Mater. Sci.* **6** 15–50
[27] Henkelman G, Uberuaga B P and Jónsson H J T 2000 A climbing image nudged elastic band method for finding saddle points and minimum energy paths *J. Chem. Phys.* **113** 9901–4
[28] Perdew J P, Burke K and Ernzerhof M 1996 Generalized gradient approximation made simple *Phys. Rev. Lett.* **77** 3865
[29] Taylor J, Guo H and Wang J 2001 *Ab initio* modeling of quantum transport properties of molecular electronic devices *Phys. Rev. B* **63** 245407
[30] Soler J M, Artacho E, Gale J D, García A, Junquera J, Ordejón P and Sánchez-Portal D 2002 The SIESTA method for *ab initio* order-N materials simulation *J. Phys. Condens. Matter* **14** 2745
[31] Troullier N and Martins J L 1991 Efficient pseudopotentials for plane-wave calculations *Phys. Rev. B* **43** 1993
[32] Hong J *et al* 2015 Exploring atomic defects in molybdenum disulphide monolayers *Nat. Commun.* **6** 6293
[33] Li X D, Wang B Q, Chen N K and Li X B 2022 Conductive mechanism in memristor at the thinnest limit: The case based on monolayer boron nitride *Appl. Phys. Lett.* **121** 073505
[34] Ren X Y, Xia S, Li X B, Chen N K, Wang X P, Wang D, Chen Z G, Zhang S and Sun H B 2018 Non-phase-separated 2D B–C–N alloys via molecule-like carbon doping in 2D BN: atomic structures and optoelectronic properties *Phys. Chem. Chem. Phys.* **20** 23106–11
[35] Si C, Choe D, Xie W, Wang H, Sun Z, Bang J and Zhang S 2019 Photoinduced vacancy ordering and phase transition in $MoTe_2$ *Nano Lett.* **19** 3612–7
[36] Yuan S, Luo X, Chan H L, Xiao C, Dai Y, Xie M and Hao J 2019 Room-temperature ferroelectricity in $MoTe_2$ down to the atomic monolayer limit *Nat. Commun.* **10** 1775
[37] Papadopoulos S, Agarwal T, Jain A, Taniguchi T, Watanabe K, Luisier M, Emboras A and Novotny L 2022 Ion migration in monolayer MoS_2 memristors *Phys. Rev. Appl.* **18** 014018
[38] Banerjee W 2020 Challenges and applications of emerging nonvolatile memory devices *Electronics* **9** 1029
[39] Banerjee W, Kashir A and Kamba S 2022 Hafnium oxide (HfO_2)—a multifunctional oxide: a review on the prospect and challenges of hafnium oxide in resistive switching and ferroelectric memories *Small* **18** 2107575
[40] Farronato M, Melegari M, Ricci S, Hashemkhani S, Bricalli A and Ielmini D 2022 Memtransistor devices based on MoS_2 multilayers with volatile switching due to Ag cation migration *Adv. Electron. Mater.* **8** 2101161
[41] Ansh and Shrivastava M 2022 Superior resistance switching in monolayer MoS2 channel-based gated binary resistive random-access memory via gate-bias dependence and a unique forming process *J. Phys. D: Appl. Phys.* **55** 085102
[42] Wu X, Ge R, Chen P A, Chou H, Zhang Z, Zhang Y, Banerjee S, Chiang M H, Lee J C and Akinwande D 2019 Thinnest nonvolatile memory based on monolayer h-BN *Adv. Mater.* **31** 1806790